Computer Aided Surgery

ISSN: 1092-9088 (Print) 1097-0150 (Online) Journal homepage: https://www.tandfonline.com/loi/icsu20

Accuracy of Muscle Moment Arms Estimated from MRI-Based Musculoskeletal Models of the Lower Extremity

Allison S. Arnold, Silvia Salinas, Deanna J. Hakawa & Scott L. Delp

To cite this article: Allison S. Arnold, Silvia Salinas, Deanna J. Hakawa & Scott L. Delp (2000) Accuracy of Muscle Moment Arms Estimated from MRI-Based Musculoskeletal Models of the Lower Extremity, Computer Aided Surgery, 5:2, 108-119, DOI: 10.3109/10929080009148877

To link to this article: https://doi.org/10.3109/10929080009148877

Computer Aided Surgery 5:108–119 (2000)

Biomedical Paper

Accuracy of Muscle Moment Arms Estimated from MRI-Based Musculoskeletal Models of the Lower Extremity

Allison S. Arnold, Ph.D., Silvia Salinas, M.S., Deanna J. Asakawa, M.S., and Scott L. Delp, Ph.D.
Biomechanical Engineering Division, Mechanical Engineering Department, Stanford University

ABSTRACT Objective: Biomechanical models that compute the lengths and moment arms of soft tissues are broadly applicable to the treatment of movement abnormalities and the planning of orthopaedic surgical procedures. The goals of this study were to: (i) develop methods to construct subject-specific biomechanical models from magnetic resonance (MR) images, (ii) create models of three lower-extremity cadaveric specimens, and (iii) quantify the accuracy of muscle-tendon lengths and moment arms estimated using these models.

Materials and Methods: Models describing the paths of the medial hamstrings and psoas muscles for a wide range of body positions were developed from MR images in one joint configuration by defining kinematic models of the hip and knee, and by specifying "wrapping surfaces" that simulate interactions between the muscles and underlying structures. Our methods for constructing these models were evaluated by comparing hip and knee flexion moment arms estimated from models of three specimens to the moment arms determined experimentally on the same specimens. Because a muscle's moment arm determines its change in length with joint rotation, these comparisons also tested the accuracy with which the models could estimate muscle-tendon lengths over a range of hip and knee motions.

Results: Errors in the moment arms calculated with the models, averaged over functional ranges of hip and knee flexion, were less than 4 mm (within 10% of experimental values).

Conclusion: The combination of MR imaging and graphics-based musculoskeletal modeling provides an accurate and efficient means of estimating muscle-tendon lengths and moment arms in vivo. Comp Aid Surg 5:108–119 (2000). ©2000 Wiley-Liss, Inc.

Key words: **musculoskeletal model, magnetic resonance imaging, muscle, moment arm, hip, knee**

INTRODUCTION

Surgeons frequently lengthen "tight" muscles in persons with cerebral palsy in an attempt to improve ambulation.[4,24] For example, children who walk with excessive flexion of their knees often have their hamstrings lengthened in an effort to diminish the crouched posture, increase the efficiency of movement, and prevent the progression of deformities. Exaggerated hip flexion during walking is commonly treated by surgical lengthening of the psoas muscle at the pelvic brim. Unfortunately, the outcomes of soft-tissue procedures to correct crouch gait and other movement abnormalities in persons with neuromuscular disorders are unpredictable and sometimes unsatisfactory.[24] We

Address correspondence/reprint requests to: Scott L. Delp, Biomechanical Engineering Division, Mechanical Engineering Department, Stanford, CA 94305-3030; Telephone: (650) 723-1230; Fax: (650) 725-1587; E-mail: delp@leland.stanford.edu.

believe that analyses of the muscle-tendon lengths during movement may help distinguish patients who have short muscles from those who do not have short muscles, and thus may provide a more effective means to identify candidates who would benefit from surgery.

Several investigators have used a generic model of the lower extremity, representing the musculoskeletal geometry of an average-sized adult male, to estimate the lengths of the hamstrings and psoas muscles during normal and crouch gait.[11,25,35,38] These studies have provided some useful clinical insights. However, it is not clear how variations in size, age, or bone geometry affect the accuracy of muscle-tendon length calculations. Children with cerebral palsy frequently exhibit deformities of the femur.[4] If these deformities substantially alter the moment arms (i.e., the lever arm, or mechanical advantage of a muscle at a joint) of muscles about the hip, then estimates of the muscle-tendon lengths calculated with a generic model may be inaccurate or misleading. Before generic musculoskeletal models can be used to guide patient-specific treatment decisions, the accuracy of the models must be tested. Hence, techniques to accurately and non-invasively characterize muscle lengths and moment arms of individual subjects need to be developed.

Muscle moment arms have been estimated in vivo from computed tomography[28,30] and from magnetic resonance (MR) images.[32,37] However, using static images alone to determine the lengths and moment arms of muscles for the wide range of body positions assumed during walking would require extensive imaging protocols to capture the muscle and joint geometry in many limb configurations. The combination of MR imaging and graphics-based musculoskeletal modeling provides a tractable alternative for estimating muscle-tendon lengths and moment arms in living subjects. For instance, a three-dimensional (3D) surface reconstruction of a limb in one joint configuration can be animated by characterizing the geometric relationships between the muscles and bones, specifying the joint kinematics, and defining how the muscle-tendon paths change with joint rotation. Murray et al.[29] (elbow joint), Cohen et al.[10] (patellofemoral joint), and others[7,9] have demonstrated the feasibility of this approach, though only Murray et al. have reported the accuracy of the muscle moment arms estimated with their MRI-based kinematic model.

In this study, we examined the accuracy with which subject-specific models of musculoskeletal geometry can be constructed from a minimal set of MR images. Graphics-based models of three lower-extremity cadaveric specimens were developed, each from approximately 250 static MR images. These models describe the geometry of the pelvis, femur, and proximal tibia, the kinematics of the hip and tibiofemoral joints, and the paths of the surrounding muscles. The accuracy of the models was evaluated by comparing hip and knee flexion moment arms estimated from the models of the specimens to the moment arms determined experimentally on the same specimens. Because the moment arm of a muscle determines its change in length with joint rotation,[1] these comparisons provided a rigorous test of the accuracy with which the models could estimate the muscle-tendon lengths and moment arms over a range of hip and knee motions. Results are presented for three muscles that are commonly lengthened to treat movement abnormalities in persons with cerebral palsy: the semimembranosus and semitendinosus muscles, which comprise the medial hamstrings, and the psoas muscle. Representation of these muscles is challenging because the hamstrings cross the knee, a joint with complex kinematics, and the psoas wraps over multiple underlying structures, including the pelvic brim and hip capsule.

METHODS

Musculoskeletal models of three lower-extremity cadaveric specimens (Table 1) were developed from several series of static MR images. The process of creating each model consisted of six steps (Figs. 1–2). Step 1 was to acquire the MR images. Step 2 was to identify and outline the anatomical structures of interest in each image, which included the pelvis, femur, tibia, psoas, semitendinosus, and semimembranosus. Step 3 was to generate 3D surface reconstructions of each structure based on the two-dimensional (2D) outlines. Step 4 was to register the surfaces from adjacent series of images, thus generating an accurate representation of each specimen's anatomy in one limb position. Step 5 was to scale kinematic models of the hip and knee to each specimen based on the bone surface geometry. Step 6 was to specify the muscle-tendon paths for functional ranges of joint motion. The resulting graphics-based models were capable of estimating muscle moment arms through ranges of hip and knee angles corresponding to walking.

Imaging Protocol

Five or six series of T1-weighted spin-echo images (TR = 400 ms, TE = 17 ms, 256 × 256, FOV = 20–24 cm for series 1–5 and 40–48 cm for series

Table 1. Skeletal Dimensions of Lower Extremity Specimens

	Specimen 1*	Specimen 2†	Specimen 3†
Maximum superior-inferior dimension of pelvis	13.8	15.0	13.8
Medial-lateral dimension between right and left ASIS* or between ASIS and midline†	10.8	22.4	24.1
Maximum anterior-posterior dimension of pelvis	15.3	15.5	15.0
Superior-inferior dimension from greater trochanter to lateral epicondyle	36.5	36.8	39.5
Maximum medial-lateral dimension of distal femur	7.7	8.7	8.9
Maximum anterior-posterior dimension of lateral condyle	6.4	6.9	6.9
Maximum medial-lateral dimension of proximal tibia	7.0	7.9	8.0
Maximum anterior-posterior dimension of proximal tibia	5.0	6.1	5.8

All measurements in units of centimeters.
* Hemipelvis specimen
† Full pelvis specimen

6) were obtained for each specimen using a 1.5T Signa MR scanner (GE Medical Systems, Milwaukee, WI) at the Children's Memorial Medical Center in Chicago (Fig. 1A). These imaging parameters enhanced the brightness of fatty tissue, which generally formed the boundaries around the muscles of interest. The specimen was placed in the prone position with the hip and knee slightly flexed (15–25°). To define the bone and muscle surface geometry, three series of transverse images were obtained using a body coil. In the first series of images, contiguous 3-mm slices were acquired from the anterior superior iliac spine (ASIS) to just below the lesser trochanter of the femur. A series of 10-mm slices were obtained along the shaft of the femur, and a series of 3-mm slices were taken from the distal femur to the proximal tibia. To capture the articular surfaces of the femur and tibia and to help define the tibiofemoral kinematics, two series of sagittal images were acquired using an extremity coil. These images were taken in 3-mm intervals at two different knee positions. A sixth series of images was obtained for the full pelvis specimens. Transverse images spanning the width of the pelvis were acquired in 3-mm slices from just above the ASIS to just below the ASIS. This facilitated definition of a medial-lateral axis for the pelvis.

Surface Reconstruction and Registration

We manually outlined the boundaries of the bones and muscles in each image slice. Each boundary was represented as a series of points that were fit with a cardinal spline. Three-dimensional surface models were generated by connecting adjacent contours of each structure with a polygonal mesh (Nuages, INRIA, France). The surface models were imported into a graphics-based musculoskeletal modeling package, SIMM.[14]

Surfaces constructed from overlapping series of transverse images were registered based on careful inspection of the bone and muscle surface geometry. These transformations were straightforward to calculate because the specimen was not moved between acquisition of the transverse series and the tapered geometry of the muscles provided sufficient constraints.

Surfaces of the femur and tibia constructed from the transverse series were registered to the corresponding surfaces created from the sagittal images to obtain a complete representation of the articular surface geometry. These transformations were calculated using an iterative closest point formulation[3] and a nonlinear least-squares algorithm (MATLAB Optimization Toolbox, The Mathworks, Natick, MA). The result of our two-step registration procedure was a 3D representation of each specimen's anatomy at the limb position in which the specimen was scanned (Fig. 1B).

Incorporation of Joint Kinematics

Coordinate systems were established for the pelvis, femur, and tibia based on anatomical landmarks. The medial-lateral axis of the pelvis coordinate system was defined by the vector from the right ASIS to the left ASIS (full pelvis specimens) or using the ASIS and midline points on the pubic symphysis and sacrum (hemipelvis specimen). The frontal plane was defined by the ASIS and the pubic tubercle. For the femur, the superior-inferior axis was defined by the vector joining the midpoint between the medial and lateral epicondyles and the center of the femoral head. The frontal plane was defined to be parallel to the vector joining the medial and lateral epicondyles. The tibia coordinate system was specified to be coincident with the femur coordinate system when the knee was fully extended.

Kinematic descriptions of the hip and tib-

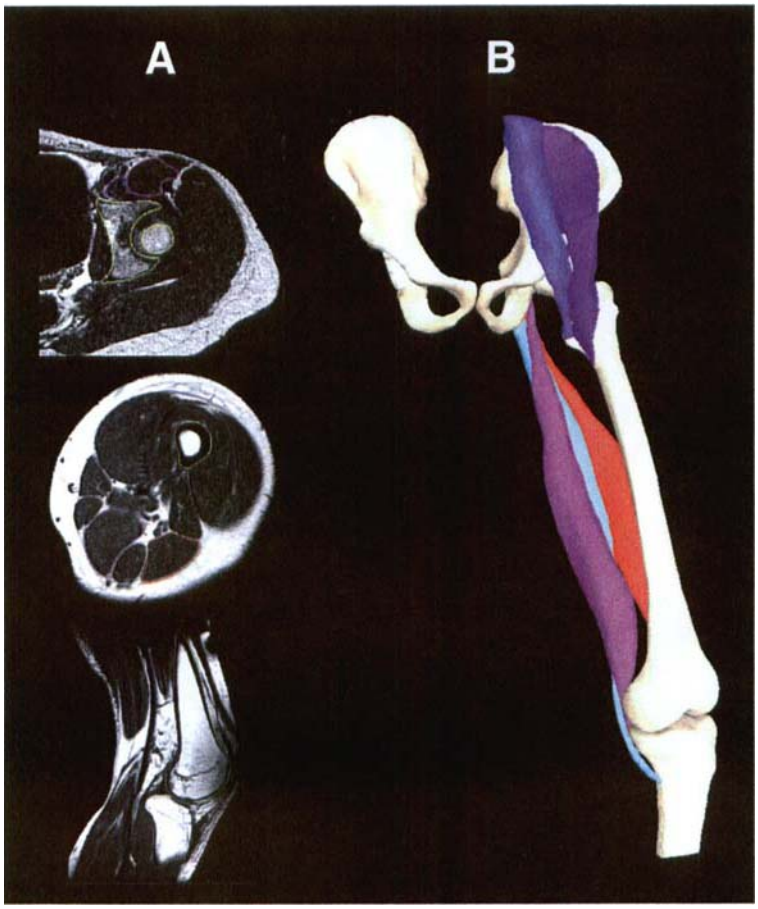

Fig. 1. Three-dimensional surface reconstruction from MR images. Surface models of the bones and muscles were generated from two-dimensional outlines that were defined manually in each image (A). Surfaces from overlapping series were registered to obtain a representation of the specimen's anatomy at one limb position (B).

iofemoral joints were defined for each model based on the specimen's bone surface geometry (Fig. 2A). The hip was assumed to be a ball-and-socket joint, and the hip center was located by fitting a sphere to the surface of the femoral head using a Gauss-Newton nonlinear least-squares algorithm (MATLAB Optimization Toolbox, The Mathworks, Natick, MA). We determined the relative positions of the femoral head and acetabulum from the scanned position. The hip joint was defined as three successive body-fixed rotations of the femur relative to the pelvis, in the order flexion, adduction, and then rotation.

The knee joint specified the 3D translations and rotations of the tibia relative to the femur as functions of knee flexion angle, and was based on published experimental measurements of tibiofemoral kinematics.[39] The femoral and tibial coordinate systems specified by Walker et al.[39] were based on the relative positions of the bones at full knee extension; however, our specimens were imaged with some degree of flexion. Also, Walker et al. reported tibiofemoral translations that had been scaled to a "nominal-sized" adult knee and averaged for 23 specimens. However, the knees of our specimens varied in size and shape. For this reason, we developed an iterative procedure to estimate, for each specimen, (i) the knee flexion angle at the scanned position and (ii) an appropriate scale factor which, when multiplied by the tibiofemoral translations specified by Walker et al., produced tibiofemoral contact locations that were consistent with published experimental data.[31] The scale factor was adjusted at each iteration such that the model's tibiofemoral contact points more closely approximated the data of Nisell et al.[31] with minimal penetration or gapping. Since the relative positions of the femur and tibia were known from the image data at one or more angles of knee flexion, the scaled knee kinematics at every iteration were

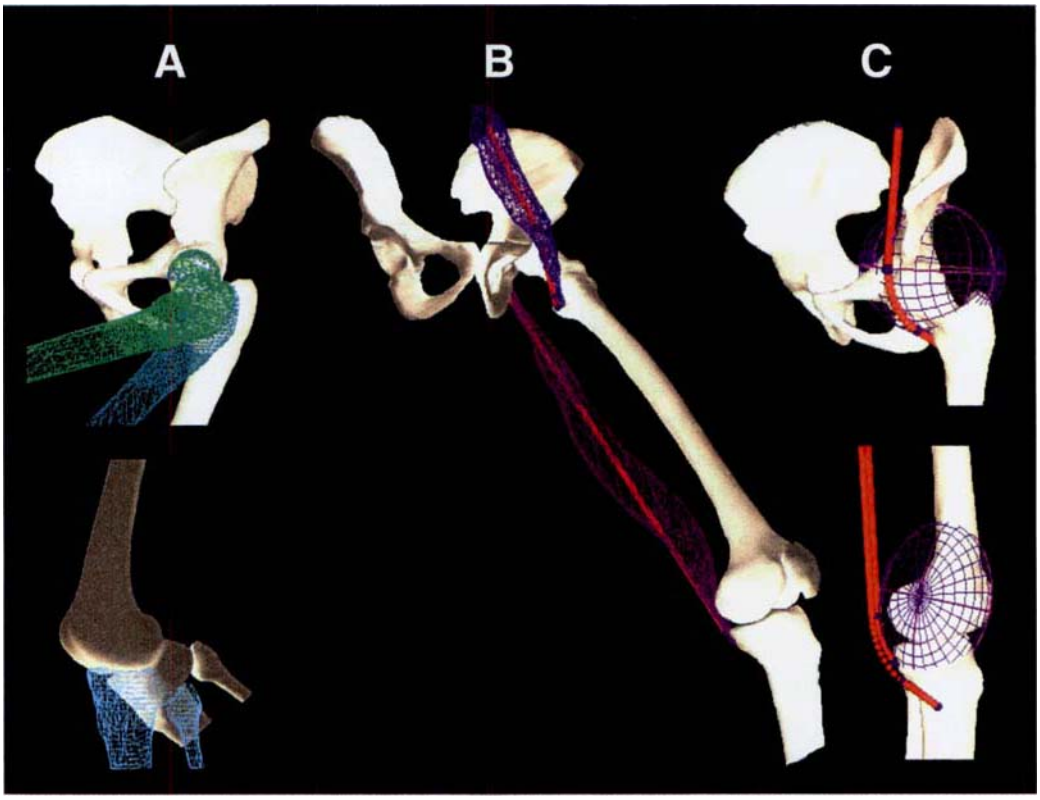

Fig. 2. Definition of joint kinematics and muscle-tendon paths. Kinematic models of the hip and knee (A) were scaled to each model based on the bone surface geometry. Attachment sites for the psoas and medial hamstrings were defined according to the 3D surface models (B). Ellipsoidal wrapping surfaces (C) were used to prescribe how the psoas muscle wrapped over the pelvic brim and hip joint capsule, and how the medial hamstrings wrapped over the gastrocnemius and posterior femoral condyles.

computed and evaluated based on these reference positions. The resulting tibiofemoral joint for each model prescribed the 3D motions of the tibia relative to the femur from 0° (extension) to 120° (flexion).

Specification of Muscle-Tendon Paths

The paths of the psoas and medial hamstrings were represented by a series of line segments. For each muscle, we developed an algorithm to (i) define the muscle attachments, and (ii) specify ellipsoidal wrapping surfaces and via points[15] to represent underlying structures and other anatomical constraints. The attachments were defined from the 3D muscle surfaces at the scanned position (Fig. 2B). Because the lumbar vertebrae were not imaged, the origin for the psoas was placed in the center of the muscle surface at the most proximal image. A via point, representing the "effective" origin of the psoas, was fixed at the pelvic brim. The origin of each of the medial hamstrings was located at the approximate centroid of the intersection of the muscle surface with the ischial tuberosity. We used a wrapping surface to characterize how the psoas muscle curves over the pelvic brim and hip joint capsule before inserting onto the lesser trochanter (Fig. 2C). A via point was added to the path of the psoas proximal to its insertion to prevent the path from penetrating the femoral neck with hip internal rotation. For each of the medial hamstrings, a wrapping surface was defined to prescribe how the muscle wraps around the posterior femoral condyles and the gastrocnemius muscle with knee extension (Fig. 2C). A via point was added proximal to the insertion of the semitendinosus to simulate the constraints produced by surrounding connective tissues.

Evaluation of Models Using Tendon Excursion Measurements

Hip flexion-extension and knee flexion moment arms were determined experimentally for the three specimens using the tendon excursion method.[1] This involved measuring the length changes of the

psoas, semimembranosus, and semitendinosus muscles through a range of hip and knee flexion. The muscle moment arms were computed as the partial derivative of the muscle-tendon lengths with respect to joint angle.

Each specimen was prepared by removing the skin and freeing the muscles of interest from extraneous soft tissue and fascia. We preserved tissues in the popliteal region that influenced the medial hamstrings' paths. The hip joint capsule and the knee ligaments were left intact to maintain normal joint motion.

Screws were drilled into landmarks on the pelvis, femur, and tibia to establish the anatomical coordinate systems for each segment. A 3D localizer (FlashPoint 5000, Image Guided Technologies, Boulder, CO) was used to digitize these landmarks and to track the positions and orientations of infrared emitter triads that were rigidly attached to the bones.

The specimen's hip center was located relative to the pelvis by slowly moving the femur through a range of flexion-extension and abduction-adduction motions, tracking the midpoint between the medial and lateral epicondyles, and fitting a sphere to these points. A Gauss-Newton nonlinear least-squares algorithm (MATLAB Optimization Toolbox, The MathWorks, Natick, MA) was used to determine the center and radius of the sphere. The center of the sphere was assumed to represent the hip center.

Each specimen was mounted in a custom-designed jig that provided control of hip flexion, adduction, rotation, and knee flexion (Fig. 3). Accurate calculation of the muscle moment arms required careful alignment of the specimen. The pelvis was oriented such that its medial-lateral axis was perpendicular to the baseplate of the jig. The pelvis was fixed to the jig using cortical bone screws (EBI Medical Systems, Parsippany, NJ). Additional bone screws and Ilizarov components[8] were used to secure the femur to a cart. The cart was equipped with one precision ball caster and two rigid casters, which were mounted on adjustable plates. The plates of the cart were angled such that the cart rolled in a circular arc. The rotation axis of the cart was collinear with the specimen's hip center. Custom software was written (LabVIEW, National Instruments Corporation, Austin, TX) and used in combination with the 3D localizer to guide the alignment process. Hip flexion and knee flexion angles were monitored during the experiment by tracking the locations of emitter triads mounted to the pelvis, femur, and tibia. Hip adduction and rotation angles were secured at 0°.

Each specimen's tibiofemoral kinematics were measured by recording the 3D translations and rotations of the tibial reference frame relative to the femoral reference frame during passive knee flexion and extension. Fourth-order polynomials were fit to the kinematics data ($R^2 > 0.98$).

To measure the length changes of the muscles, polyester suture was sewn to the distal tendon of each muscle, routed through a suture anchor at the muscle's origin, and connected to a Celesco PT101 position transducer (Celesco Transducer Products, Canogo Park, CA). For the psoas, the suture was secured proximal to the pelvic brim to permit wrapping over anatomical structures. The transducer applied a constant tension of 7.5 N, and was reported to be accurate to within 0.15 percent of full scale, or ± 0.38 mm. The data were sampled at 15 Hz using a 16-bit analog-to-digital converter (PCI-MIO-16XE-50, National Instruments Corporation, Austin, TX). The A/D board determined

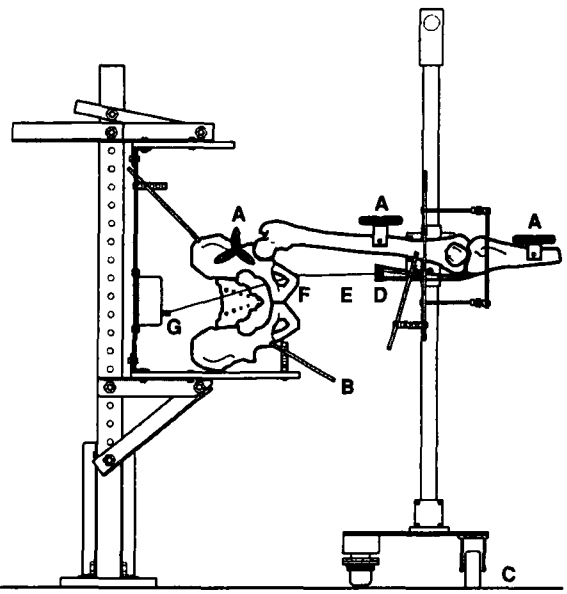

Fig. 3. Experimental set-up for tendon excursion measurements. Infrared emitter triads were mounted to the pelvis, femur, and tibia to track joint angles (A). The pelvis was mounted to the baseplate with cortical bone screws (B). The femur was secured to a cart. The wheels of cart (C) rolled in a circular arc about the specimen's hip center to flex the hip. Tendon excursion measurements were made by sewing a wire mesh (D) to the muscle, attaching suture (E) to the wire mesh, routing the suture through a suture anchor (F) at the muscle's origin, and connecting the suture to a position transducer (G).

the resolution of the measurements, which was 0.04 mm.

The length changes of the muscles were recorded while slowly moving the hip or knee joint through the maximum attainable range of motion. To determine hip flexion-extension moment arms, the tibia was secured with the knee in extension, and the cart was rolled through a range of hip flexion (generally 80°). To determine knee flexion moment arms, the cart was secured with suction cups with the hip at 0° flexion, and the knee was manually rotated through a range of knee flexion (generally 70°). Five trials were collected for each muscle at each joint. Before each set of trials, the limb was taken through the range of motion in an effort to eliminate muscle stretching during data collection.

Fourth-order polynomials were fit to each trial of tendon excursion vs. flexion angle data ($R^2 > 0.99$). The moment arms for each trial were calculated by taking the first derivatives of the polynomial fits. The average moment arm curves and standard deviations across trials were computed.

The average moment arm curves determined from the excursion data were compared with the moment arms predicted from the MRI-based model of the corresponding specimen. An average error was computed for each muscle and specimen by calculating the average, over the range of motion achieved during the experiment, of the absolute difference between the experimentally determined moment arm and the calculated moment arm, expressed in millimeters and as a percentage of the experimental moment arm.

RESULTS

Hip flexion-extension moment arms for the psoas and medial hamstrings calculated with the models compared favorably with the experimental data. For the psoas (Fig. 4), the average errors between the experimentally determined moment arms and the calculated moment arms ranged from 1.1 mm, or 5% of the experimental moment arms (Specimen 1), to 2.7 mm (8%, Specimen 3). For the semimembranosus (Fig. 5), the hip extension moment arm errors ranged from 1.0 mm (2%, Specimen 2) to 3.8 mm (9%, Specimen 3). For the semitendinosus, the average errors ranged from 1.3 mm (2%, Specimen 3) to 2.5 mm (4%, Specimen 2).

The knee flexion moment arms for the medial hamstrings calculated with the models were within 10% of the experimental data (Fig. 6). The average knee flexion moment arm errors for the semimembranosus ranged from 0.1 mm (< 1%, Specimen 1) to 3.5 mm (10%, Specimen 2). The average errors for the semitendinosus ranged from 1.8 mm (5%, Specimen 1) to 3.9 mm (9%, Specimen 2).

DISCUSSION

Knowledge of muscle-tendon lengths and moment arms is important for planning interventions aimed at the correction of walking abnormalities because tight muscles that restrict movement are often surgically lengthened. Lengthening of the medial hamstrings and psoas muscles, for example, often improves the posture and limb alignment of persons with cerebral palsy who walk with a troublesome, crouched gait. However, unnecessary lengthening of these muscles can leave patients with weak, dysfunctional legs. Previous studies, based on computer models representing normal adult musculoskeletal geometry, have suggested that analyses of the muscle-tendon lengths during walking may be helpful for deciding if a muscle should be surgically lengthened.[11,25,35,38] These generic models must be tested — and the accuracy of the predicted muscle-tendon lengths verified — before such models can be used to guide treatment decisions for specific patients.

In this study, we (i) developed methods to create subject-specific musculoskeletal models from MR images, (ii) constructed models of three lower-extremity specimens, and (iii) quantified the accuracy with which hip and knee flexion moment arms of the medial hamstrings and psoas muscles could be estimated using these models. We showed that the moment arms computed with the three specimen-specific models were within 10% of the moment arms determined experimentally on the specimens.

To evaluate the significance of these moment arm errors for predicting the length changes of the muscles during movement, we calculated the corresponding errors in the length changes of the muscles for 60° ranges of hip and knee flexion, and we compared these errors to variations in the peak muscle-tendon lengths determined for eighteen unimpaired subjects during walking. This comparison is relevant because muscle-tendon lengths of cerebral palsy patients are often compared to averaged data from unimpaired subjects to determine if a muscle is shorter or longer than normal during walking.[11,35,38] The 60° range of flexion was chosen because it represents a functional range of hip and knee angles during normal and crouch gait.[11] The means and standard deviations of the peak lengths for the unimpaired subjects were estimated

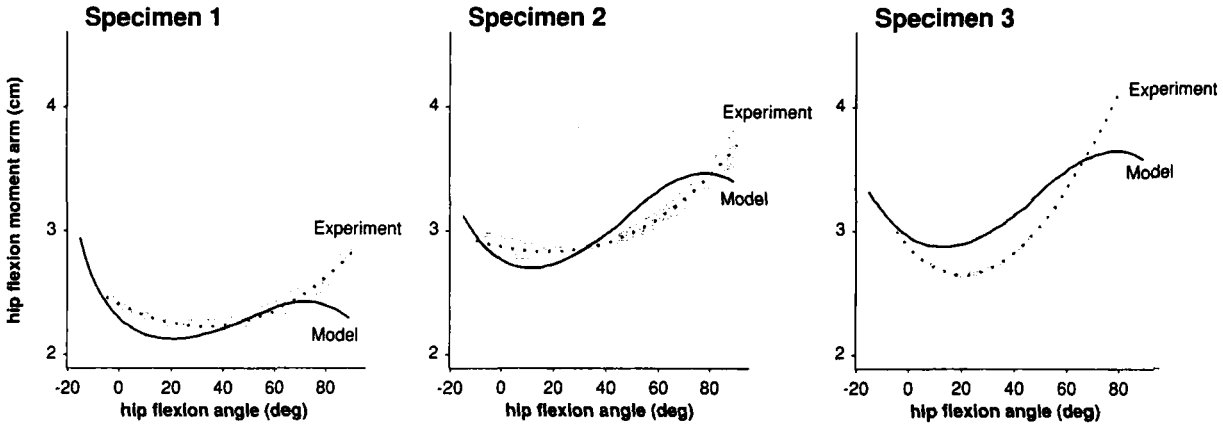

Fig. 4. Hip flexion moment arms of the psoas for Specimens 1, 2, and 3. The moment arms estimated from the MRI-based models (solid lines) are compared with the moment arms determined experimentally (mean ± one standard deviation, shaded regions).

using each specimen-specific model in conjunction with the subjects' measured gait kinematics. We calculated the length change of the psoas from the muscle's effective origin at the pelvic brim to its insertion on the lesser trochanter. Hence, we assumed that changes in psoas length due to rotations at the lower lumbar spine and lumbosacral joint were negligible.

The maximum errors in the estimated length changes of the psoas, semimembranosus, and semitendinosus were 2.5 mm, 2.1 mm, and 3.7 mm, respectively (Fig. 7). These errors are less than one standard deviation of the peak muscle-tendon lengths for the group of unimpaired subjects. Based on these data, we believe that our methods for constructing musculoskeletal models from MR images are sufficiently accurate for estimating the length changes of these muscles in vivo. Our next step is to develop subject-specific models of children with cerebral palsy. Insights gained from these studies will help evaluate and improve existing musculoskeletal models and, ultimately, may facilitate the design of improved treatment strategies for persons with neuromuscular disorders.

The procedures we used to develop and evaluate the MR-based musculoskeletal models in this study have some important limitations. First, we assumed that the hip could be well represented by a ball-and-socket joint. Hip flexion and extension moment arms calculated with the three specimen-specific models compared favorably with the experimental data (Figs. 4 and 5). This suggests that

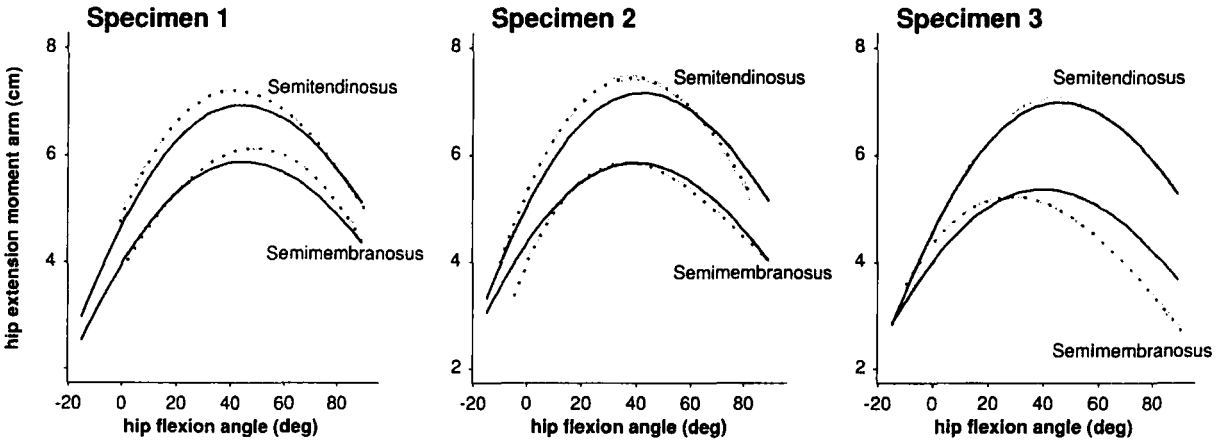

Fig. 5. Hip extension moment arms of the medial hamstrings for Specimens 1, 2, and 3. The moment arms estimated from the MRI-based models (solid lines) are compared with the moment arms determined experimentally (mean ± one standard deviation, shaded regions).

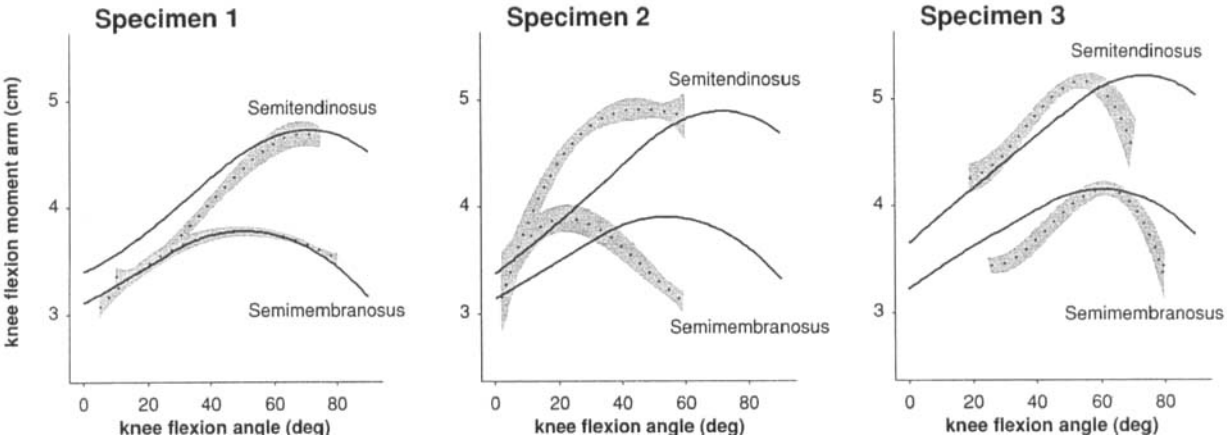

Fig. 6. Knee flexion moment arms of the medial hamstrings for Specimens 1, 2, and 3. The moment arms estimated from the MRI-based models (solid lines) are compared with the moment arms determined experimentally (mean ± one standard deviation, shaded regions).

our model of hip kinematics and our methods for locating the hip center were adequate—at least for the specimens in this study. However, some individuals with cerebral palsy have hips that are subluxed or dislocated. Additional work may be required to develop accurate representations of deformed hips, and to determine how these deformities alter the lengths and moment arms of muscles.

Second, knee motions in the models were based on published measurements of tibiofemoral kinematics,[39] which we scaled to each specimen's bones. To determine whether the moment arms of the medial hamstrings were influenced by our choice of scale factor, we performed a sensitivity study.[33] Varying the scale factor by ± 0.2 (a feasible tolerance) changed the knee flexion moment arms of the medial hamstrings by at most 1.1 mm. Altering the "assumed" knee flexion angle at the scanned position by ± 4° changed the moment arms by at most 1.7 mm. Because these changes are small (< 5%) compared to the moment arms of the muscles, we believe our iterative method for choosing a scale factor was satisfactory.

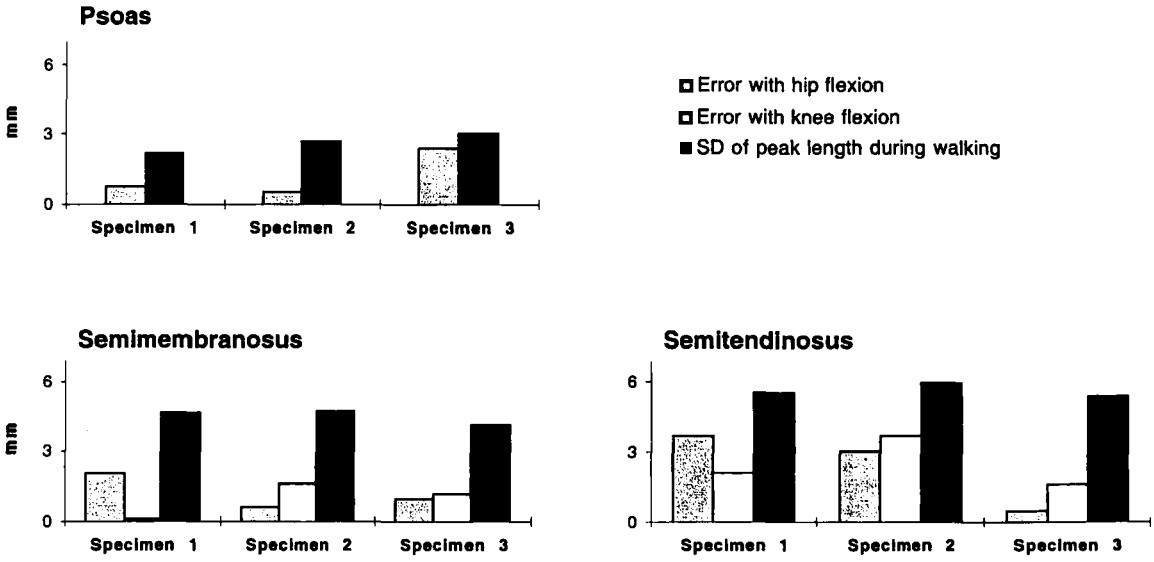

Fig. 7. Maximum errors in the estimated length changes of the muscles compared to variations in the peak muscle-tendon lengths during normal walking. Note that errors in the hip (shaded bars) and knee (open bars) are always less than one standard deviation of the peak lengths during normal walking (filled bars).

It is possible that our knee model would not prescribe accurate motions of the tibiofemoral joint for children with cerebral palsy, even after scaling the model to a child's bone geometry. In fact, the kinematic equations reported by Walker et al.[39]—which represent the averaged knee motions of 23 adult specimens—may not characterize the tibiofemoral kinematics of many unimpaired adults. We found that the knee flexion moment arms of the medial hamstrings for Specimen 2 were consistent in magnitude with the experimental data, but were shifted in joint angle by about 30° (Fig. 6b). Using our experimental measurements of tibiofemoral kinematics, we determined that this discrepancy could be attributed primarily to differences between the measured and the prescribed tibiofemoral motions (Fig. 8). Fortunately, the length changes of the medial hamstrings calculated with the model of Specimen 2 were nearly as accurate as the length changes computed with the other models, despite errors in the tibiofemoral kinematics (Fig. 7). This suggests that predictions of the muscle length changes may be relatively insensitive to errors in the prescribed knee motions. In future studies, the acquisition of cine phase-contrast MR images,[36] or static MR images at many angles of knee flexion, may enable better, more individualized descriptions of tibiofemoral kinematics to be developed.

Third, we represented the muscles in our MRI-based models as a series of line segments, and we designed the muscle-tendon paths based on image data from only the scanned limb position. We used ellipsoidal wrapping surfaces to simulate interactions between the muscles and the underlying structures, and we restricted each muscle to interact with only one wrapping surface. There are several limitations to this approach. For example, we defined a wrapping surface to simulate wrapping of the psoas over the pelvic brim and hip capsule with hip extension, and we used a via point[15] to keep the muscle from penetrating the femoral neck with hip internal rotation. This strategy worked well for large ranges of hip flexion and rotation, but was effective only for very small ranges of hip abduction or adduction. Similarly, a wrapping surface at the distal femur prevented the semimembranosus and semitendinosus from penetrating the femoral condyles with knee extension, but there was no way to also keep these muscles from penetrating the ischium at large angles of hip flexion. If the lengths or moment arms of these muscles need to be evaluated for a wider range of joint angles than are used during walking, then algorithms that allow muscles to wrap over multiple surfaces need to be developed. Detailed studies of how the muscle-tendon paths change with joint configuration in vivo could also improve the reliability of kinematic models constructed from static images.

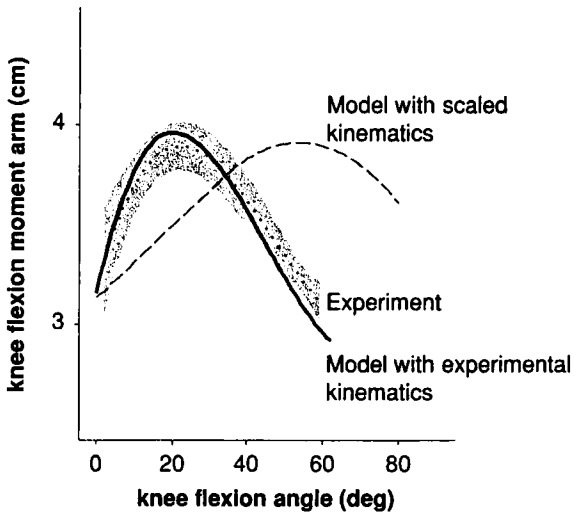

Fig. 8. Comparison of knee flexion moment arms calculated using the scaled tibiofemoral kinematics (dashed line) and the measured kinematics (solid line) for the semimembranosus of Specimen 2. The knee flexion moment arms for this specimen more closely match the experimentally determined moment arms (shaded region) when estimated using a model that prescribes the measured kinematics.

Finally, we evaluated our methods for creating the subject-specific models by comparing muscle moment arms calculated with the models of three specimens to the moment arms determined experimentally on the specimens, but there are several potential sources of error in these measurements. Stretching of the muscle-tendon-suture complex or small inaccuracies in specimen alignment, for example, could have caused errors in our tendon excursion versus joint angle data. To gain confidence in our experimentally determined moment arms, we compared these moment arms to moment arms published in the literature.

Buford et al.[6] measured knee flexion moment arms in fifteen specimens and reported the averaged moment arm curves and standard deviations for each of the hamstring muscles. Peak knee flexion moment arms of the medial hamstrings for the three specimens in our study were within one standard deviation (within 4 mm) of the peak moment arms that Buford et al. reported. Hence, we are reasonably confident in the knee flexion moment arms determined from our experiments.

At the hip, a comprehensive set of published moment arm data for comparison was not available.

In the most widely-cited study of hip moment arms to date, Dostal et al.[20,21] estimated muscle attachment sites from skeletal landmarks on one dry bone specimen. The corresponding moment arms of the hamstrings and psoas muscles were presented, but only for the upright position. The hip extension moment arms of the medial hamstrings for the three specimens in our study were slightly smaller than these data, with differences ranging from 3 to 9 mm. The hip flexion moment arms of the psoas for the specimens in our study were 6 to 11 mm greater than these data. This discrepancy may have been due to wrapping of the psoas over the underlying structures in our experiments, which would not have been accounted for in the dry bone study of Dostal et al. Hence, the muscle moment arms determined for the three specimens in our study provide more accurate estimates than previously available in the literature.

The techniques described in this paper for creating subject-specific musculoskeletal models from MR images are applicable to a wide range of orthopaedic surgical procedures. Surgeons frequently introduce changes in muscle force- and moment-generating capacities by modifying the lengths or moment arms of muscles. Predicting the biomechanical consequences of surgical alterations, therefore, requires detailed knowledge of the muscle-tendon lengths and moment arms before and after surgery. Generic models of musculoskeletal geometry have been used to simulate tendon lengthenings,[18,19] tendon transfers,[7,17,22,27] osteotomies[2,5,12,23,34] and hip reconstructions.[13,16,26] These studies have determined how variations in surgical parameters affect musculotendon lengths, moment arms, force-generating capacities, and joint contact forces post-operatively — important data for surgical planning. However, no study has reported how variations in musculoskeletal geometry across patients might influence the simulation results. We believe that the development of accurate, time-effective, and cost-effective methods to construct subject-specific biomechanical models from image data could have tremendous impact on the design, planning, and evaluation of a variety of musculoskeletal procedures.

ACKNOWLEDGMENTS

We are grateful to Peter Loan and Ken Smith for help with development of the modeling software; Emil Davchev, Norman Fung, JoAnn Mason, Wendy Murray, Mahi Durbhakula, and Erik King for assistance with data collection and analysis. Special thanks to Carolyn Moore, Stephen Vankoski, Claudia Kelp-Lenane, Julie Witka, and Tony Weyers of the Motion Analysis Center, Children's Memorial Medical Center in Chicago, for providing the gait data. This work was performed in the Departments of Biomedical Engineering and Physical Medicine & Rehabilitation at Northwestern University, and in the Sensory Motor Performance Program at the Rehabilitation Institute of Chicago. We gratefully acknowledge funding from NIH Grant R01 HD33929, the United Cerebral Palsy Foundation, and an NSF Graduate Research Fellowship to S. Salinas.

REFERENCES

1. An KN, Takahashi K, Harrigan TP, Chao EY. Determination of muscle orientations and moment arms. J Biomech Eng 1984;106:280–282.
2. Benvenuti JF, Rakotomanana L, Leyvraz PF, Pioletti DP, Heegaard JH, Genton MG. Displacements of the tibial tuberosity. Clin Orthop Rel Res 1997;343:224–234.
3. Besl PJ, McKay ND. A method for registration of 3-D shapes. IEEE Trans Pat Anal Mach Int 1992;14:239–256.
4. Bleck EE. Orthopaedic Management in Cerebral Palsy. 2nd edition. London: Mac Keith Press; 1987.
5. Brand RA, Pedersen DR. Computer modeling of surgery and a consideration of the mechanical effects of proximal femoral osteotomies. In: The Hip: Proceedings from the 12th Open Scientific Meeting of the Hip Society. St. Louis: CV Mosby; 1984.
6. Buford WL, Ivey FM, Malone JD, Patterson RM, Peare GL, Nguyen DK, Stewart AA. Muscle balance at the knee: moment arms for the normal knee and the ACL-minus knee. IEEE Trans Rehab Eng 1997;5:367–379.
7. Buford WL, Thompson DE. A system for three-dimensional interactive simulation of hand biomechanics. IEEE Trans Biomed Eng 1987;34:444–453.
8. Catagni MA, Malzev V, Kirienko A. Advances in Ilizarov Apparatus Assembly. Maiocchi AB, editor. Milan, Italy: Medicalplastic srl; 1996.
9. Chao EYS, Lynch JD, Vanderploeg MJ. Simulation and animation of musculoskeletal joint system. J Biomech Eng 1993;115:562–568.
10. Cohen ZA, McCarthy DM, Roglic H, Henry JH, Rodkey WG, Steadman JR, Mow VC, Ateshian GA. Computer-aided planning of patellofemoral joint OA surgery: developing physical models from patient MRI. In: Wells WM, Colchester A, Delp S, editors: Proceedings of the First Annual Conference on Medical Image Computing and Computer-Assisted Intervention (MICCAI'98). Lecture Notes in Computer Science 1496. Berlin, Heidelberg, New York: Springer-Verlag; 1998. p 9–20.
11. Delp SL, Arnold AS, Speers RA, Moore CA. Hamstrings and psoas lengths during normal and crouch

gait: implications for muscle-tendon surgery. J Orthop Res 1996;14:144–151.
12. Delp SL, Bleck EE, Zajac FE, Bollini G. Biomechanical analysis of the Chiari pelvic osteotomy: preserving hip abductor strength. Clin Orthop Rel Res 1990;254: 189–198.
13. Delp SL, Komattu AV, Wixson RL. Superior displacement of the hip in total joint replacement: effects of prosthetic neck length, neck-stem angle, and anteversion angle on the moment-generating capacity of the muscles. J Orthop Res 1994;12:860–870.
14. Delp SL, Loan JP. A graphics-based software system to develop and analyze models of musculoskeletal structures. Comp Bio Med 1995;25(1):21–34.
15. Delp SL, Loan JP, Hoy MG, Zajac FE, Topp EL, Rosen JM. An interactive graphics-based model of the lower extremity to study orthopaedic surgical procedures. IEEE Trans Biomed Eng 1990;37:757–767.
16. Delp SL, Maloney W. Effects of hip center location on the moment-generating capacity of the muscles. J Biomech 1993;26:485–499.
17. Delp SL, Ringwelski DA, Carroll NC. Transfer of the rectus femoris: effects of transfer site on moment arms about the knee and hip. J Biomech 1994;27:1201–1211.
18. Delp SL, Statler K, Carroll NC. Preserving plantar flexion strength after surgical treatment for contracture of the triceps surae: a computer simulation study. J Orthop Res 1995;13:96–104.
19. Delp SL, Zajac FE. Force- and moment-generating capacity of lower-extremity muscles before and after tendon lengthening. Clin Orthop Rel Res 1992;284: 247–259.
20. Dostal WF, Andrews JG. A three-dimensional biomechanical model of hip musculature. J Biomech 1981; 14:803–812.
21. Dostal WF, Soderberg GL, Andrews JG. Actions of hip muscles. Phys Ther 1986;66:351–361.
22. Dul J, Shiavi R, Green NE. Simulation of tendon transfer surgery. Eng Med 1985;14(1):31–38.
23. Free SA, Delp SL. Trochanteric transfer in total hip replacement: effects on the moment arms and force-generating capacities of the hip abductors. J Orthop Res 1996;14:245–250.
24. Gage JR. Gait Analysis in Cerebral Palsy. London: Mac Keith Press; 1991.
25. Hoffinger SA, Rab GT, Abou-Ghaida H. Hamstrings in cerebral palsy crouch gait. J Ped Orthop 1993;13: 722–726.
26. Johnston RC, Brand RA, Crowninshield RD. Reconstruction of the hip. J Bone Joint Surg 1979;61-A(5): 639–652.
27. Lieber RL, Friden J. Intraoperative measurement and biomechanical modeling of the flexor carpi ultaris-to-extensor carpi radialis longus tendon transfer. J Biomech Eng 1997;119:386–391.
28. McGill SM, Patt N, Norman RW. Measurement of the trunk musculature of active males using CT scan radiography: implications for force and moment generating capacity about the L4/L5 joint. J Biomech 1988; 21:329–341.
29. Murray WM, Arnold AS, Salinas S, Durbhakula M, Buchanan TS, Delp SL. Building biomechanical models based on medical image data: an assessment of model accuracy. In: Wells WM, Colchester A, Delp S, editors: Proceedings of the First Annual Conference on Medical Image Computing and Computer-Assisted Intervention (MICCAI'98). Lecture Notes in Computer Science 1496. Berlin, Heidelberg, New York: Springer-Verlag; 1998. p 539–549.
30. Nemeth G, Ohlsen H. In vivo moment arm lengths for hip extensor muscles at different angles of hip flexion. J Biomech 1985;18:129–140.
31. Nisell R, Nemeth G, Ohlsen H. Joint forces in extension of the knee. Acta Orthop Scand 1986;57:41–46.
32. Rugg SG, Gregor RJ, Mandelbaum BR, Chiu L. In vivo moment arm calculations at the ankle using magnetic resonance imaging (MRI). J Biomech 1990;23: 495–501.
33. Salinas S. Evaluation of Musculoskeletal Models Derived from Magnetic Resonance Images. M.S. thesis. Evanston, IL: Northwestern University; 1999.
34. Schmidt DJ, Arnold AS, Carroll NC, Delp SL. Length changes of the hamstrings and adductors resulting from derotational osteotomies of the femur. J Orthop Res 1999;17:279–285.
35. Schutte LM, Hayden SW, Gage JR. Lengths of hamstrings and psoas muscles during crouch gait: effects of femoral anteversion. J Orthop Res 1997;15:615–621.
36. Sheehan FT, Zajac FE, Drace JE. Using cine phase contrast magnetic resonance imaging to non-invasively study in vivo knee dynamics. J Biomech 1998; 31:21–26.
37. Spoor CW, van Leeuwen JL. Knee muscle moment arms from MRI and from tendon travel. J Biomech 1992;25:201–206.
38. Thompson NS, Baker RJ, Cosgrove AP, Corry IS, Graham HK. Musculoskeletal modelling in determining the effect of botulinum toxin on the hamstrings of patients with crouch gait. Dev Med Child Neurol 1998;40:622–625.
39. Walker PS, Rovick JS, Robertson DD. The effects of knee brace hinge design and placement on joint mechanics. J Biomech 1988;21:965–974.